Arabian Journal of Chemistry (2020) 13, 8684–8696

King Saud University

Arabian Journal of Chemistry

www.ksu.edu.sa
www.sciencedirect.com

ORIGINAL ARTICLE

Utilization of biowaste as an eco-friendly biodegradable corrosion inhibitor for mild steel in 1 mol/L HCl solution

Venkatesan Hemapriya [a,1], Mayakrishnan Prabakaran [b,1], Subramanian Chitra [a], Manoharan Swathika [a], Seung-Hyun Kim [b], Ill-Min Chung [b,*]

[a] *Department of Chemistry, PSGR Krishnammal College for Women, Coimbatore 641 004, Tamil Nadu, India*
[b] *Department of Crop Science, College of Sanghuh Life Science, Konkuk University, Seoul 05029, South Korea*

Received 11 August 2020; accepted 29 September 2020
Available online 22 October 2020

KEYWORDS

Biowaste;
Corrosion;
Mild steel;
SEM;
EDX;
AFM

Abstract This report focuses on the application of a biodegradable biowaste [human hair-(HHR)], to produce a mild steel corrosion inhibitor. The performance of HHR extract in inhibiting metallic corrosion in 1 mol/L HCl was investigated. The analysis of the metal corrosion behavior using electrochemical and weight loss techniques revealed that HHR exhibits an efficient corrosion-mitigating effect via adsorption on the metal surface following a Langmuir isotherm. Tafel-plot results revealed the mixed-mode corrosion protection behavior of HHR. Surface analysis using scanning electron microscopy (SEM), energy-dispersive X-ray spectroscopy (EDX), atomic force microscopy (AFM), and Fourier transform infrared (FT-IR) spectroscopy provided evidence for the precipitation of a protective HHR film on the metal surface.

1. Introduction

Iron and its alloys, including mild steel, are applied in many industrial fields such as oil production and refining, chemical and petrochemical manufacture, ore and fertilizer production, desalination, power stations, automobile, and architectural applications not only as a prime and engineering material, but also as a constructional material (Atia and Saleh, 2003). Mild steel exhibits good mechanical and structural properties, high technological significance, high thermal conductivity, good environmental stability, corrosion resistance, and a relatively low cost (Saeed et al., 2003; Bentiss et al., 2000). To protect industrial metallic materials, pretreatments and maintenance practices such as pickling and cleaning are often employed (Anadebe et al., 2018). The aggressive acids used in the pickling and cleaning operations often tend to promote the corrosion of metallic structures, and if not suitably protected, steel can progressively lose its desirable properties due to such

* Corresponding author.
E-mail address: imcim@konkuk.ac.kr (I.-M. Chung).
[1] Venkatesan Hemapriya and Mayakrishnan Prabakaran have contributed equally to this work.
Peer review under responsibility of King Saud University.

ELSEVIER Production and hosting by Elsevier

https://doi.org/10.1016/j.arabjc.2020.09.060

treatments (Rehim et al., 2001). Corrosion scientists have employed preventive approaches including the application of corrosion inhibitors (Al-Otaibi et al., 2014), use of paint systems containing corrosion inhibitors (Mansfeld and Tsai, 1991), and cathodic protection (Abreu et al., 1999), to inhibit or control metal corrosion. Among these, the use of corrosion inhibitors is the most practical, simple, and cost-effective technique. Inorganic compounds, such as phosphates, nitrites, arsenates, tetraborates, and chromates, as well as organic compounds with heteroatoms and/or multiple bonds and polymers, have been used as corrosion inhibitors (Hemapriya et al., 2017; Abdallah et al., 2012). Traditional inorganic inhibitors oxidize the metal surface to form an impervious film that impedes aggressive agents in the environment from reaching the metal, while organic inhibitors adsorb onto the metal surface via heteroatoms, such as S, N, and O atoms; aromatic ring π electrons; and multiple bonds (Salasi et al., 2007; Hemapriya et al., 2016). In recent times, the suitability of organic and inorganic inhibitors has been actively debated in terms of their bio-toxicity, hazardous heavy metal content, non-biodegradability, and expressivity. Most reports describe polymers as moderate inhibitors that are not cost effective (Rajeswari et al., 2013). Thus, the selection of an effective corrosion control material or strategy must take into account not only the strength of the protection provided, but also the total cost of operation, toxicity, biodegradability, and environmental hazards of the materials involved. Thus, researchers have become increasingly interested in green corrosion inhibitors.

Easily biodegradable, non-hazardous, and relatively inexpensive plant extracts have been reported to act as efficient metal corrosion inhibitors (Rajeswari et al., 2014; Ocampo et al., 2015; Oguzie et al., 2012; Umoren et al., 2013). We have explored the use of *Epipremnum aureum* (Prabakaran et al., 2018), *Chaenomeles sinensis* (Chung et al., 2018), *Aster koraiensis* (Prabakaran et al., 2017), *Rhus verniciflua* (Prabakaran et al., 2016a), *Cryptostegia grandiflora* (Prabakaran et al., 2016b), *Ligularia fischeri* (Prabakaran et al., 2016c), and *Tragia plukenetii* (Prabakaran et al., 2016d), as corrosion inhibitors for mild steel in acid media. Recently, systemic thinking and the utilization of biowaste materials have become increasingly popular in the scientific community. Shrimp waste protein (Farag et al., 2018), coconut coir dust extract (Umoren et al. 2012), and rice straw extract (Mahross et al., 2016) have been reported as corrosion inhibitors for different metals in acid media. Another biowaste resource is human hair, which comprises the hard fibrous protein keratin, lipids, and the pigment melanin (Verma et al., 2016). Human hair is found in the municipal waste streams of almost all towns and cities worldwide. Leachate from waste including human hair can create eutrophication problems, while burning hair produces a foul odor and toxic gases. The ideal way to address the perennial problem of hair waste disposal would be to develop products or systems that utilize human hair as a resource. To date, hair has been used in fertilizer, oil spill remediation, construction material reinforcement, oil filtration, amino acid extraction, textile and fiber stuffing, molded furniture and objects, and heavy metal removal applications (Zheljazkov et al., 2008; Murthy et al., 2004; Gupta, 2008; Gupta, 2014). Additionally, the use of human hair is being researched in areas as diverse as concrete reinforcement (Akhtar and Ahmad, 2009), tissue regeneration (Yoo et al., 2010), biomaterials engineering (Hirao et al., 2005), superconducting system composites (Michael et al., 2010), catalytic nanoparticle platforms (Deng et al., 2016), suturing material (Eroğlu et al., 2003), and microelectrodes (Xu et al., 2009). However, to the best of our knowledge, human hair extract (HHR) containing the pigment melanin and lipids has not been explored as an inhibitor for any metal in acid media.

The present work aims to reduce the corrosion of mild steel in HCl using an extract of human hair in a mixed solvent consisting of methanol, ethanol, and chloroform (40:30:30 v/v). The pigment melanin and the lipids present in human hair are extracted using this solvent system (Nakamura et al., 2002; Gopiraman et al., 2017). Melanin contains heteroatoms such as O, N, and S, which are the potential reactive sites in reported organic inhibitors. Based on these properties, we have attempted to exploit this abundant renewable biowaste resource. The corrosion inhibition performance of HHR was analyzed using gravimetric, electrochemical and surface examination approaches.

2. Materials and techniques

2.1. Mild steel specimen

The mild steel rods used in the weight loss and surface examination studies contained 0.079% C, 0.025% P, 0.018% Mn, and 0.021% S, with the remainder being Fe, and had dimensions of 3.0 × 1.0 × 0.5 cm. For the electrochemical analysis, mild steel rods with the above composition encapsulated in Teflon with an unprotected area of 0.785 cm^2 were used. Prior to each experiment, the metal specimens were polished to a mirror finish using emery sheets of different grades, washed with double-distilled water, degreased using acetone, air-dried, and stored as suggested by ASTM G1 - 03(2017)e1 (Standard Practice for Preparing, Cleaning, and Evaluating Corrosion Test Specimens). The corrosive electrolyte (1 mol/L HCl) were prepared by diluting 37.0% HCl in distilled water and standardized.

2.2. Human hair extract preparation

Black human hair collected from a saloon shop in Coimbatore, Tamil Nadu, India, was washed sequentially with distilled water and ethanol and dried. The human hair was cut into small pieces and ball-milled to obtain a fine powder. Approximately 5 g of the powdered human hair was soaked in 250 mL of a methanol, ethanol, and chloroform (40:30:30 v/v) mixture for seven days, after which the mixture was filtered.

2.3. Gravimetric method

The pre-weighed, mirror-polished mild steel rods were suspended in 100 mL of the aggressive electrolyte (1 mol/L HCl) containing various HHR concentrations. After a 3 h immersion period, the specimens were removed, washed, dried, and re-weighed using an ACCULAB Electronic top-loading analytical balance. The weight loss inhibition efficiency η (%), surface coverage (θ) and corrosion rate (C_r) were calculated as,

$$\eta(\%) = \frac{(W_0 - Wi)}{(W_0)} \times 100 \quad (1)$$

$$C_r = 87.6 \ \ W/Atd \quad (2)$$

$$\theta = \frac{\eta(\%)}{100} \quad (3)$$

where W_0 and W_i are the weight loss of the metal sheet exposed to the inhibitor-free acid and the corresponding HHR-containing acid, respectively, and W is the weight loss. A, t, and d represent the exposed area of the metal rod in cm^2, exposure time in h, and density of the mild steel in g/cm^3, respectively. To analyze the impact of temperature on the efficiency of HHR, the same gravimetric technique was performed at 303, 313, 323, and 333 ± 1 K using 100 ppm of HHR.

2.4. Electrochemical techniques

Electrochemical measurements were conducted in an Ivium compact-stat electrochemical measurement unit. Impedance and polarization measurements were carried out using a classical three-electrode Pyrex glass cell setup with a capacity of 100 mL. A platinum wire and a mild steel rod with an exposed surface area of 0.785 cm^2 were employed as the counter electrode and working electrode, respectively. All the potential data were recorded with reference to the saturated calomel electrode. Prior to each measurement, the mild steel working electrode was immersed in the test electrolyte at the open circuit potential (OCP) to attain the stable state.

2.4.1. Electrochemical impedance spectroscopy study

AC impedance measurements were performed at corrosion potentials over the frequency range 0.01 Hz−10 KHz with 25 mV peak-to-peak voltage excitation per second. The electrochemical resistance, R_t, and double layer capacitance, C_{dl}, were computed from the Z_{real} vs $Z_{imaginary}$ plot. From the R_t data, the inhibition efficiency of HHR was calculated using the formula,

$$\eta(\%) = \frac{(R_{ct} - R'_{ct})}{(R_{ct})} \times 100 \quad (4)$$

where R_{ct} and R'_{ct} are the electrochemical resistance in the presence and absence of HHR.

2.4.2. Polarization technique

The Tafel polarization measurements were executed immediately after electrochemical impedance spectroscopy (EIS) at a sweep rate of 1 mV/sec over the potential range from −200 mV to + 200 mV relative to the open circuit potential. The corrosion potential, E_{corr}, corrosion current, I_{corr}, and slopes of the cathodic and anodic Tafel curves, b_c and b_a, were determined using the software package Ivium Soft. The inhibition efficiency (Tan et al., 2020; Tan et al., 2019) was computed as,

$$\eta(\%) = \frac{(i'_{corr} - i_{corr})}{(i'_{corr})} \times 100 \quad (5)$$

where i_{corr} and i'_{corr} refer to the corrosion current with and without HHR.

2.5. Surface investigation studies

2.5.1. Scanning electron microscopy-energy dispersive X-ray spectrometry and atomic force microscopy

The surface morphology of the corroded and protected mild steel specimens were scanned using a scanning electron microscope (SEM, JEOL-Model JSM - 6390) equipped to perform energy dispersive X-ray spectrometry (EDX). Atomic force micrographic examination of metal specimens immersed in the HHR-containing electrolyte and the inhibitor-free electrolyte were performed using a multimode surface probe microscope (NTMDT, NTEGRA Prima, Russia) with a force constant of 0.36–6.06 N/m.

2.5.2. Fourier transform infrared spectroscopy

The inhibitor film adsorbed on the surface of the mild steel rods was analyzed by subjecting the rods to Fourier transform infrared (FT-IR) spectral analysis using an IR Affinity-1 (Shimadzu, Japan) before and after treatment with a 100 ppm concentration of HHR for three hours.

3. Results and discussion

3.1. Mechanism of metal weight loss

The electrochemistry of metal corrosion involves anodic dissolution of the metal and cathodic hydrogen evolution as described in the following reactions:

$$\text{At anode} \quad Fe \rightarrow Fe^{2+} + 2e^- \quad (6)$$

$$\text{At cathode} \quad 2H^+ + 2e^- \rightarrow H_{2(g)} \quad (7)$$

$$\text{Overall reaction} \quad Fe + 2H^+ \rightarrow Fe^{2+} + H_2 \quad (8)$$

With reference to the above equations the corrosion rate of the metal can be determined by gravimetric methods such as measurement of the metal weight loss, hydrogen evolution, dissolved Fe^{2+} concentration, and change in the pH of the electrolyte. Among these, the weight loss method is most widely used because of its simplicity and the reliability of the measurement; thus, it has become the baseline method in many corrosion monitoring programs (Afidah, and Kassim, 2008). In the present study, the ability of HHR to inhibit the corrosion of mild steel exposed to 1 mol/L HCl containing 0, 20, 40, 60, 80, or 100 ppm HHR at 303 ± 1 K for 3 h is presented in Table 1. Inspection of the data reveals a steady decrease in the metal corrosion rate and increase in efficiency with increasing HHR concentration. The decrease in corrosion was due to the movement of HHR components from the bulk electrolyte onto the mild steel surface, where they were adsorbed as a thin film that shielded the metal surface from the aggressive acid environment. The enhanced efficiency at 100 ppm was attributed to a greater coverage of the mild steel surface with a larger quantity of HHR components. Corrosion occurs at the unblocked active sites on the electrode surface at the electrode/acid interface; the adsorption of the HHR components

Table 1 Corrosion rate and inhibition efficiency at various concentration of HHR for mild steel corrosion in 1 mol/L HCl.

Conc. (ppm)	C_r (mmpy)	θ HCl	η %	SD[a]
Blank	115.93	–	–	–
20	60.37	0.4793	47.93	1.5
40	35.84	0.6909	69.09	1.2
60	16.61	0.8567	85.67	0.9
80	08.85	0.9237	92.37	0.8
100	03.88	0.9665	96.65	1.0

[a] SD, standard deviation.

could block these sites. HHR showed 96% efficiency in the 1 mol/L HCl medium. These results revealed that both the degree of protonation and nature of the acid anions affected the process of metal corrosion (Oguzie, 2008; Lashgari et al., 2010).

Weight loss analysis was carried out at 303 to 333 ± 1 K to analyze the effect of temperature on the corrosion inhibition efficiency. The analyses were conducted using HHR concentration of 100 ppm, as this afforded the maximum efficiency at 303 ± 1 K. No extraordinary increase in corrosion inhibition efficiency was observed above this concentration. The results provided in Fig. 1, clearly demonstrate that although HHR exhibited a corrosion mitigating effect over the entire temperature range, the efficiency decreased with increasing temperature. The corrosion of mild steel in inhibitor-free acid solutions also increased with upsurge in temperature. These results indicated that both the corrosion protective ability of HHR and the degree of metal dissolution were dependent on the temperature. The decline in efficiency could also result from the desorption of the adsorbed HHR from the electrode surface, which would suggest a physical adsorption mechanism (Antropov, 1967). The inhibition performance of the present HHR is better or comparable to (Table 2) many other inhibitors including *Rhododendron schlippenbachii* (94.24%) (Chung et al., 2020a–c), *Pachysandra terminalis* (95.79%) (Chitra et al., 2019), *Gentiana olivieri* (93.70%) (Baran et al., 2019), *Petroselium sativum* (92.39%) (Benarioua et al., 2019), *Musa paradisiac* (92%) (Ji et al., 2015), *Cryptostegia grandiflora* (87.54%) (Prabakaran et al., 2016b) and *Lannea coromandelica* (93.80%) (Muthukrishnan et al., 2017).

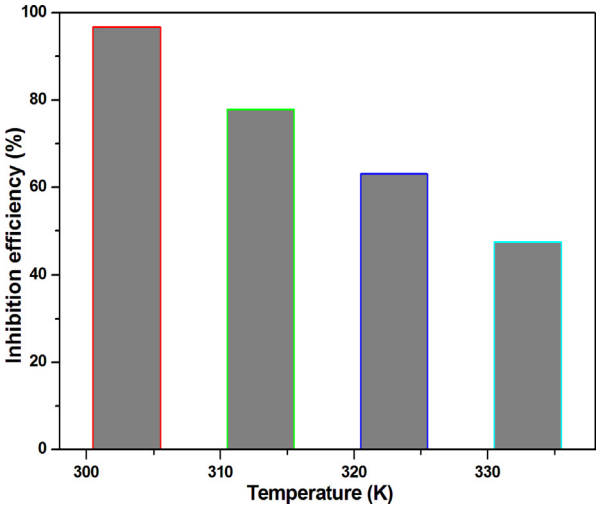

Fig. 1 Effect of temperature on the mild steel corrosion inhibition efficiency in 1 mol/L HCl.

Table 2 Comparison of HHR and other corrosion inhibitors.

S. No	Inhibitors	η (%)
1	*Rhododendron schlippenbachii*	94.24 (Chung et al., 2020a–c)
2	*Pachysandra terminalis*	95.79 (Chitra et al., 2019)
3	*Gentiana olivieri*	93.70 (Baran et al., 2019)
4	*Petroselium sativum*	92.39 (Benarioua et al., 2019)
5	*Musa paradisica*	92.00 (Ji et al., 2015)
6	HHR extract[#]	96.65
7	*Cryptostegia grandiflora*	87.54 (Prabakaran et al., 2016b)
8	*Lannea coromandelica*	93.80 (Muthukrishnan et al., 2017)

[#] Present work.

3.2. Activation and thermodynamic parameters

To gain insight into the thermodynamics of the dissolution of mild steel in the inhibitor-free acid electrolytes and those containing HHR, the Arrhenius and Eyring transition state equations, equation (9) and (10), were used:

$$Cr = Ae^{(-E_a/RT)} \tag{9}$$

$$Cr = \frac{RT}{Nh} exp\left(\frac{\Delta S^*}{R}\right) exp\left(\frac{-\Delta H^*}{RT}\right) \tag{10}$$

where E_a is the apparent activation energy of the corrosion process, R is the gas constant, A is a pre-exponential factor, h is Planck's constant, ΔS* and ΔH* represent the apparent entropy of activation and the apparent enthalpy of activation, respectively, and N is Avogadro's number. The E_a values for the corrosion process were calculated from the slopes of the linear plots of log (C_r) versus 1/T (Fig. 2), which had correlation coefficients of 0.99. The E_a values for the inhibitor-free 1 mol/L HCl (19.62 KJ mol^{-1}) is lower than the corresponding value for the HHR-containing electrolyte (94.00 KJ mol^{-1}). The higher E_a values of the HHR-containing acid solutions indicated a change in the corrosion process, with an increase in the energy barrier due to the adsorption of the inhibitor molecules on the electrode surface (Lv et al., 2015; Yadav et al., 2015). ΔH* and ΔS* were computed from the slope

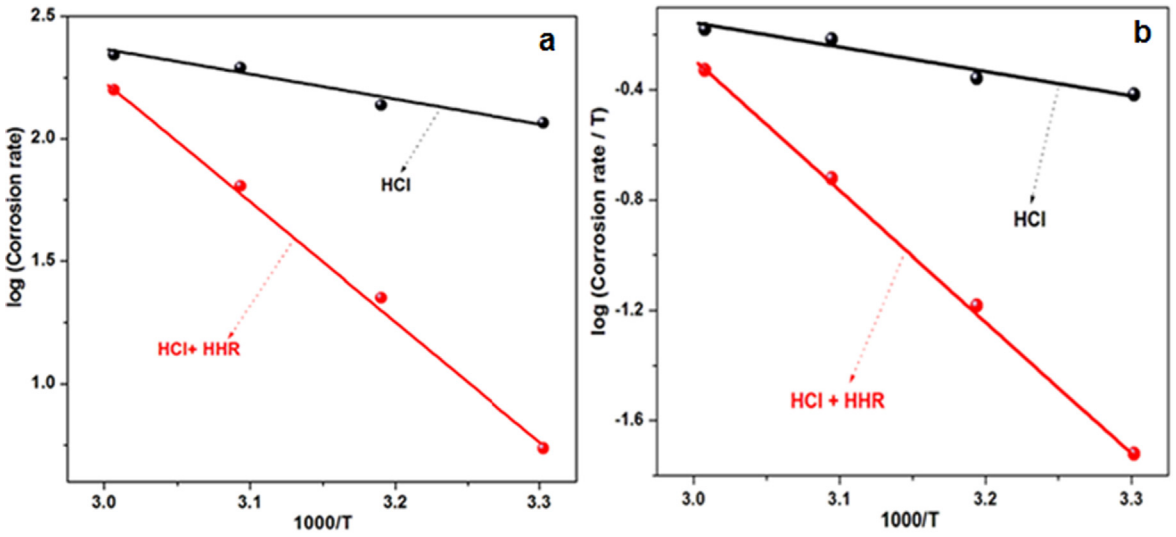

Fig. 2 a) Arrhenius plots, and b) Transition state plots for mild steel corrosion in 1 mol/L HCl in the presence and absence of HHR.

(−ΔH*/2.303R) and intercept (log (R/Nh) + (ΔS*/2.303R)) of the linear transition state plot of log (C_r/T) versus 1/T (Fig. 2b). The ΔH* values is positive for both the inhibitor-free 1 mol/L HCl (16.98 KJ mol^{-1}) and electrolyte with HHR (91.36 KJ mol^{-1}), indicative of enhanced metal dissolution rate at higher temperatures. Additionally, the more positive value of ΔH* for the HHR-inhibited solution indicated that more heat energy was required for the mild steel dissolution process, thus confirming the formation of a barrier film by the inhibitor molecules (Sangeetha et al., 2016). The ΔS* values for the inhibitor-free acid electrolyte is negative (1 mol/L HCl (−92.18 KJ mol^{-1}), implying that water molecules were uniformly adsorbed on the steel surface. The inhibited acid gave larger ΔS* values (1 mol/L HCl (128.42 KJ mol^{-1}) than the inhibitor-free analogue, which reflected the disorder resulting from the existence of different bonding interaction modes between the metal surface and inhibitor molecules (Jeeva et al., 2017).

3.3. Adsorption isotherm

According to Yesudass et al., the adsorption of an inhibitor onto the surface of a corroding metal does not reach a true equilibrium, but instead an adsorption steady state (Yesudass et al., 2016). Nevertheless, when the metal corrosion rate is small, the adsorption reaches a quasi-equilibrium state. Hence, studying the thermodynamics of this quasi-equilibrium adsorption using appropriate equilibrium isotherms is quite reasonable. Such adsorption isotherms are useful in understanding the mechanisms behind the organo-electrochemical reactions involved in the adsorption of the inhibitor on the metal surface (Bockris and Swinkells, 1964). In this study, the adsorption of HHR onto the steel surface in 1 mol/L HCl electrolyte was analyzed by the graphical fitting of the weight loss data using various adsorption isotherm models; the fits of the various models were compared using their chi-square (R^2) values. The best linear fit (Fig. 3) was obtained using the Langmuir isotherm, (equation (11)) with R^2 values of 1.000 for HCl.

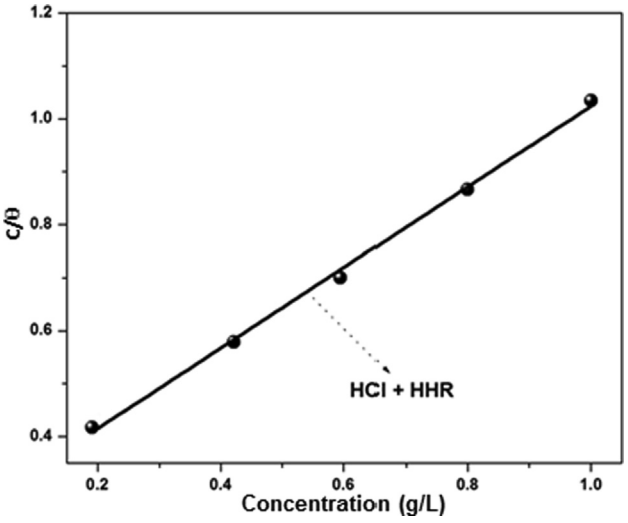

Fig. 3 Langmuir plots for corrosion of mild steel in 1 mol/L HCl.

$$C/\theta = 1/K_{ads} + C \quad (11)$$

where C and K_{ads} denote the inhibitor concentration and adsorption equilibrium constant, respectively. The K_{ads} values were computed from the intercept of the Langmuir plots (Fig. 3). The standard adsorption free energy (ΔG°_{ads}) was derived from the relationship in equation (12).

$$\Delta G^{\circ}_{ads} = -RTln(55.5K_{ads}) \quad (12)$$

The negative ΔG°_{ads} values indicated that the HHR adsorption process was spontaneous and that the adsorbed layer on the metal surface was strong and stable. According to previous reports, ΔG°_{ads} values of −20 kJ mol^{-1} or lower indicate electrostatic interaction between the charged electrode surface and charged inhibitor species (i.e., physical adsorption), while values of −40 kJ mol^{-1} or greater indicate chemical adsorption (Ali et al., 2008). The ΔG°_{ads} values for HHR adsorption in 1 mol/L HCl is −24.16 KJ mol^{-1}. This value fell between

the cutoffs −20 and −40 kJ mol^{-1}, signifying that the interaction between the inhibitor and the steel surface was not exclusively a physisorption or chemical sorption process, but instead involved a complex comprehensive type comprising both the interactions (Hassan et al., 2007; Zhang et al., 2014; Luo et al., 2017).

3.4. Electrochemical measurements

3.4.1. Electrochemical impedance spectroscopy

EIS is a sophisticated technique that is widely employed to study the corrosion behavior and adsorption phenomena of mild steel. The EIS measurements of mild steel electrodes were performed at their open circuit potential in inhibitor-free 1 mol/L HCl, as well as in electrolyte containing different concentrations of HHR. The corresponding Open Circuit Potential (OCP), Nyquist, Bode modulus, and phase angle representations of EIS are shown in Fig. 4. As shown in Fig. 4b, significant changes in the impedance response of the mild steel were observed after the addition of HHR. However, semi-circular impedance profiles were obtained at all HHR concentrations in the studied electrolyte. This indicated that the anticorrosion mechanism of HHR was similar in the studied electrolyte. The impedance spectra shows, only a single capacitive semicircle depressed at a high frequency is seen; the centers of the semi-circles deviated from the real axis. This might have been due to a decrease in C_{dl} and an increase in the charge transfer resistance. The addition of HHR increased the diameters of the semi-circular impedance profiles (Fig. 4b), with respect to the blank solution. Furthermore, the addition of HHR enhanced the magnitude of the Bode modulus and the phase angle (values) (Fig. 4(c) and (d, e)). The highest impedance values were observed for the highest studied inhibitor concentration (100 ppm), which suggested enhanced surface coverage at higher concentrations due to the greater availability of the active components of the extract for adsorption onto the steel electrode. The charge transfer resistance (R_{ct}) and double layer capacitance (C_{dl}) parameters were simulated using a simple equivalent circuit (Fig. 4b). R_{ct} indicates the degree of electron transfer across the surface, and it is inversely proportional to the corrosion rate. As shown in Table 3, the R_{ct} values increased with an increasing extract concentration, indicating a decrease in the mild steel corrosion rate and an increase in inhibition efficiency. The C_{dl} values were lower in the HHR-containing electrolyte compared with those of the inhibitor-free acid electrolyte. The decrease in the capacitance of the double layer was attributed to a reduction in the charge on the steel surface, which in turn was caused by the adsorption of a protective inhibitor film on the electrode surface and the desorption of adsorbed H_2O molecules from the surface, reducing the local dielectric constant (Chaitra et al., 2016). HHR showed 96.65% corrosion inhibition efficiency in 1 mol/L HCl. This indicated greater adsorption of the inhibitor, possibly due to the greater tendency of Cl^- ions to strongly adsorb on the steel surface. Thus, the chloride ions in HCl played a major role in the inhibition process via joint adsorption on the metal surface with HHR (Saranya et al., 2017; Yildiz and Mer, 2019).

3.4.2. Tafel polarization studies

The anodic and cathodic Tafel polarization curves provide information regarding the corrosion phenomenon and corrosion inhibition process. Inhibitors can reduce the corrosion rate by modifying the anodic and/or cathodic process. To study the effect of HHR on the corrosion process of mild steel, the anodic and cathodic polarization behaviors in 1 mol/L HCl were recorded in the presence of different inhibitor concentrations. The plots shown in Fig. 4f, demonstrate a shift in the anodic and cathodic Tafel lines towards lower corrosion current densities in the presence of the inhibitor, signifying that the added HHR impeded the anodic dissolution and consequently, decreased the H_2 evolution reaction. The associated electrochemical parameters, namely, the corrosion potential (E_{corr}), current density (I_{corr}), and the slopes of anodic and cathodic Tafel lines (b_a, b_c), derived from extrapolation of the linear segments are listed in Table 4. The displayed data show that the presence of HHR changed both the E_{corr} and I_{corr} values. The decline in the I_{corr} values in the inhibited systems compared with the non-inhibited system indicate that metal dissolution was retarded in the HHR-containing electrolyte. The analysis of the data also reveals an inverse relationship between the HHR concentration and the I_{corr} value in 1 mol/L HCl. This might have resulted from the efficient adsorption of HHR at the metal/acid electrolyte interface. The shift in E_{corr} towards the noble direction by the addition of HHR reveal greater adsorption of HHR on the anodic site. Furthermore, no consistent trend in the shifts of the corrosion potential (E_{corr}) was observed with increasing HHR concentration for HCl indicating that the inhibitor diminished both the anodic (dissolution of mild steel) and cathodic (evolution of H_2) corrosion half-cell reactions. The inhibition efficiency of HHR, as computed from the I_{corr} values, increased (Table 4) with the HHR concentration, which is consistent with the inverse relationship between I_{corr} and the inhibitor concentration. No clear relationship is observed between the Tafel slopes b_a and b_c and the HHR concentration. The lack of a trend in the cathodic and anodic slope values suggested that the mechanisms of the anodic and cathodic corrosion reactions were not modified by the addition of HHR (Kumar and Karthikeyan, 2013). According to previous reports, if the shift in the E_{corr} value of an inhibited system with respect to that observed in the inhibitor-free electrolyte is $> \pm 85$ mV, the inhibitor can be regarded as a cathodic/anodic inhibitor; otherwise, it is considered to be a mixed mode inhibitor (Oguzie, 2007; Liu et al., 2009). The differences between the E_{corr} values for mild steel in the inhibitor-free HCl and the HHR-containing counterparts were computed, and the maximum E_{corr} shifts were found to be 35.6 mV in 1 mol/L HCl. This value is smaller than the required ± 85 mV threshold, which conclude the mixed-mode corrosion inhibitive nature of HHR. HHR extract shows 85.15%, efficiency in HCl which is in accordance with that of weight loss and impedance techniques (Anitha et al., 2019; Keleşoğlu et al., 2019).

3.5. Morphological analysis of the metal surface

3.5.1. SEM and EDX studies

The examination of the surfaces of metallic specimens exposed to the inhibitor-free and HHR-containing electrolyte provided further insight into the inhibition behavior of HHR. Fig. 5 shows the SEM micrograph images of metal specimens exposed to either the inhibitor-free corrosive environment or electrolyte containing the optimum concentration (100 ppm) of HHR. The metal surfaces exposed to the inhibitor-free electrolyte was heavily damaged, while those treated with HHR-

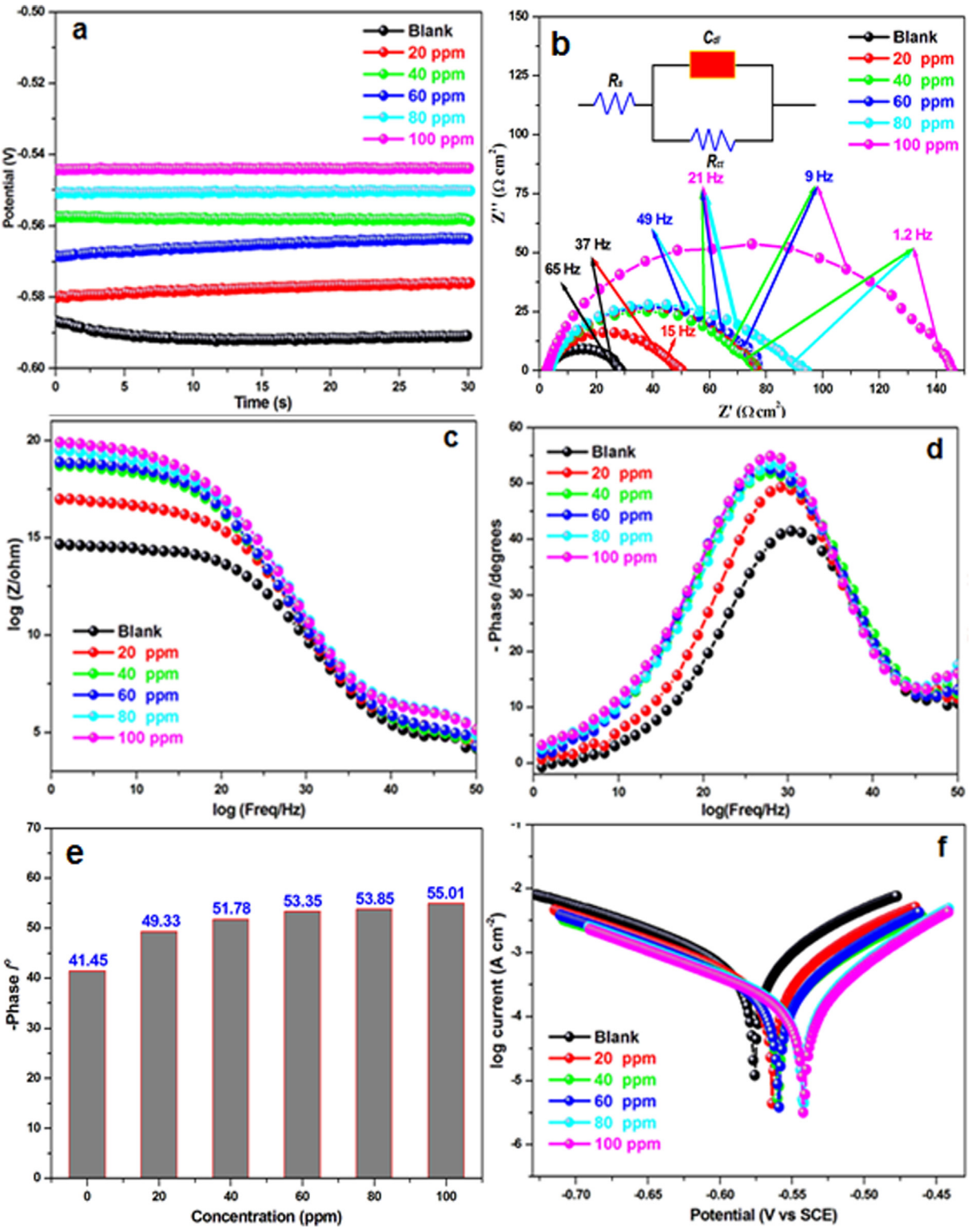

Fig. 4 a) OCP, b) Nyquist plots, c) phase plots, e) bode plots, e) phase angle values, and f) Tafel plots for mild steel in 1 mol/L HCl in the absence and presence of HHR.

containing HCl exhibited less damage with reduced surface roughness, indicating their minimal corrosion. This remarkable improvement in the surface morphology of the inhibited mild steel surface revealed that the inhibitor film adsorbed on the metal surface acted as a barrier to block access of the corrosive species to the active sites and hence mitigated corrosion (Malathy et al., 2020).

To complement the above results, the elemental compositions of the steel surfaces after exposure to 1 mol/L HCl containing either 0 or 100 ppm HHR were investigated using

Table 3 Corrosion parameters for mild steel at various concentrations of HHR by impedance method at 303 ± 1 K.

Conc. (ppm)	R_{ct} (Ω cm^2)	C_{dl} (μF/cm^2)	η (%)	SD[a]
Blank	20.77	19.5	–	–
20	38.55	19.2	46.11	1.2
40	57.26	18.8	63.71	0.9
60	67.11	17.8	69.04	0.8
80	78.42	17.1	73.50	1.5
100	139.92	16.3	85.15	1.1

[a] SD, standard deviation.

Table 4 Corrosion parameters for mild steel corrosion at various concentrations of HHR as determined using the potentiodynamic polarization method at 303 ± 1 K.

Conc. (ppm)	Tafel slopes (mV/dec)		E_{corr} (mV)	I_{corr} (μA/cm^2)	η (%)	SD[a]
	b_a	b_c				
Blank	138.7	86.4	−576.1	689.7	–	–
20	137.5	78.4	−563.5	370.78	46.24	0.6
40	142.3	87.2	−559.5	293.56	57.43	1.2
60	126.9	75.3	−559.2	252.8	63.34	0.9
80	129.7	65.6	−540.5	169.92	75.36	0.7
100	130.6	67.0	−541.6	102.8	85.09	1.1

[a] SD, standard deviation.

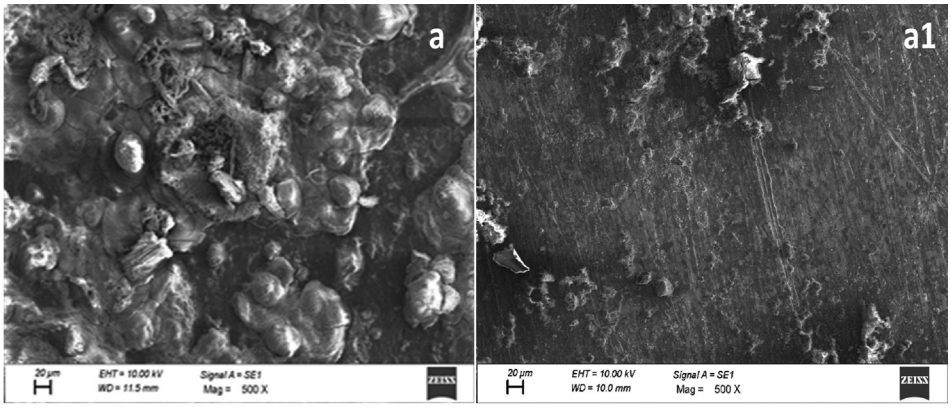

Fig. 5 SEM images of mild steel in 1 mol/L HCl in the absence (a) and presence of 100 ppm of HHR (a1).

EDX; the spectra are shown in Fig. 6. The high oxygen content, 54.05% in 1 mol/L HCl of the sample exposed to the inhibitor-free acid environment were reduced significantly by the addition of HHR 31.85% in 1 mol/L HCl. Additionally, the intensities of the Cl, S, and P signals of the inhibited metal specimen are also reduced with respect to the unprotected samples. Furthermore, the EDS spectra of the inhibitor-treated metal samples (Fig. 6) exhibited more intense N and C signals (Chung et al., 2020a–c). These results confirmed the adsorption of the inhibitor via the N and O atoms of the active components of HHR, such as the pigment melanin and lipids, as a barrier film to protect against acid attack.

3.5.2. Atomic force microscopy

Atomic force microscopy (AFM) is a nano- to micro-scale analysis technique that can also be used to study the effect of the inhibitors on metal corrosion. Two- and three-dimensional AFM profiles of steel specimens subjected to 1 mol/L HCl containing either 0 or 100 ppm HHR are depicted in Fig. 7. The topography of the uninhibited metal surface (Fig. 7) exhibits large, deep pores caused by the extensive attack of corrosive species (Unnisa et al., 2019; Mahalakshmi et al., 2019). The high roughness (55.59 nm) of the metal surfaces exposed to the inhibitor-free 1 mol/L HCl, due to the rapid and aggressive acid attack are evident from the visible the cracks, pits and corrosion products on the steel surface. The surfaces of the metal samples exposed to the electrolytes containing 100 ppm HHR exhibited uniform surface and small pits (Fig. 7), with significantly reduced surface roughness values 39.24 nm, confirming the adsorption of HHR to the metal, in accordance with the SEM results (Manokarana and Prabakaran, 2019; Anitha et al., 2020).

3.5.3. FT-IR spectral analysis

FT-IR spectroscopy was performed to confirm the SEM and AFM results. The FT-IR spectrum of HHR in Fig. 8 shows

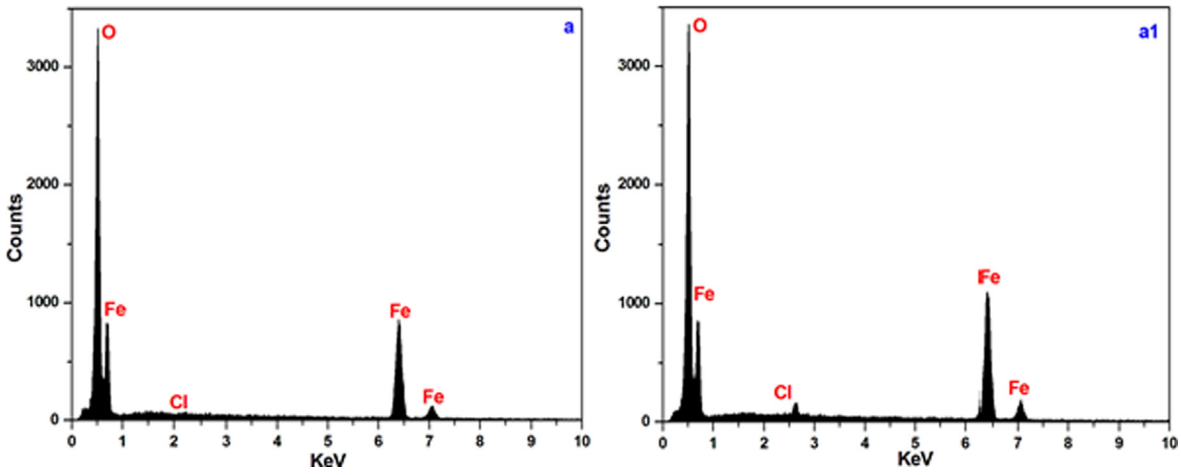

Fig. 6 EDX spectra for mild steel in 1 mol/L HCl in the absence (a) and presence of 100 ppm of HHR (a1).

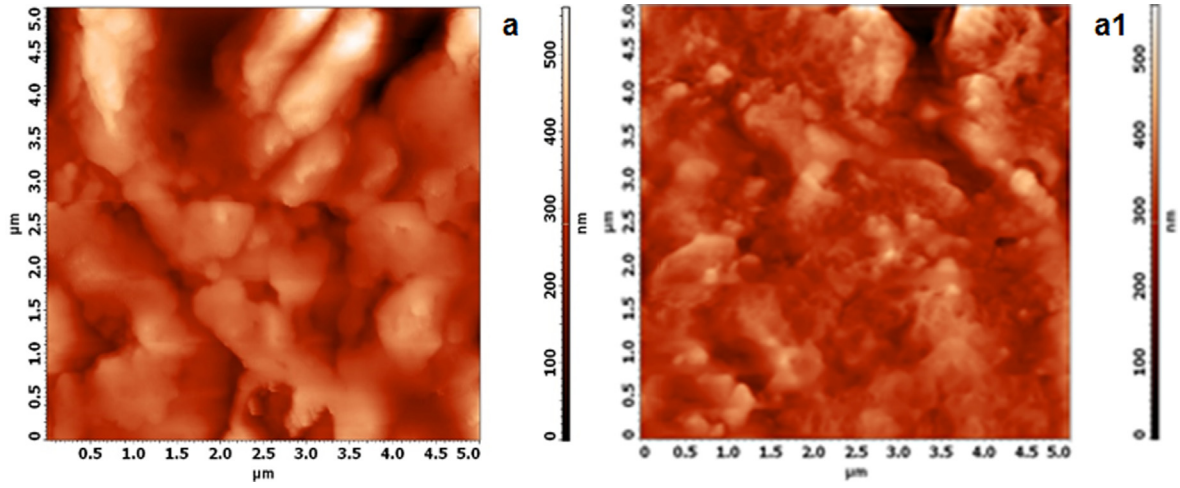

Fig. 7 AFM surface topography of mild steel in 1 mol/L HCl in the absence (a) and presence of 100 ppm of HHR (a1).

characteristic bands corresponding to the functional groups present in its active components. The absorption band at 3374 cm^{-1} originated from —OH stretching overlapped by an N-H stretching mode (Muthukrishnan et al., 2014; Mbonyiryivuze et al., 2015) this band was associated with phenolic, carboxylic acid, and aromatic amino groups present in the pyrrolic and indolic groups of melanin, which was the main constituent of HHR. The bands at 1642 cm^{-1} and 1363 cm^{-1} arose from C═O stretching vibrations and C—H stretching vibrations, respectively. A comparative analysis of the spectra of metal samples treated with 1 mol/L HCl containing 100 ppm HHR with the spectrum of HHR revealed the shift of the above-mentioned bands to higher frequency and the presence of additional bands (Chung et al., 2019). These results suggested that specific interactions had occurred between the inhibitor and the metal surface. The shift of the —OH and associated N—H bands from 3374 cm^{-1} to 3314 cm^{-1} (HCl) revealed the coordination of HHR with Fe^{2+} through the OH and amino groups of the pyrrolic and indolic groups in melanin. The shift in the C═O stretching band from 1642 cm^{-1} to 1578 cm^{-1} (HCl) also confirmed the interaction of HHR with Fe^{2+} via oxygen atoms. The above results further confirmed the absorption HHR on the metal surface.

3.6. Proposed mechanism of inhibition

From the results of the chemical and electrochemical studies, it can be concluded that the corrosion inhibition effect of HHR arose from the adsorption of the components of HHR at the electrode/electrolyte interface. Surface analysis using AFM and FT-IR, confirmed the adsorption of inhibitor molecules on the electrode surface. Previous literature has reported that inhibitor adsorption can involve physical electrostatic adsorption, chemical adsorption, or a complex combination of both (Verma and Khan, 2016; Jmiai et al., 2017; Karthik et al., 2015). In the present study, the Gibbs free energy data for adsorption supported combined electrostatic and chemical adsorption. The polarization results revealed that HHR exhibited mixed-mode inhibition behavior. In HCl solutions, the active components of HHR exist as neutral molecules or cationic species (protonated HHR). The neutral HHR components

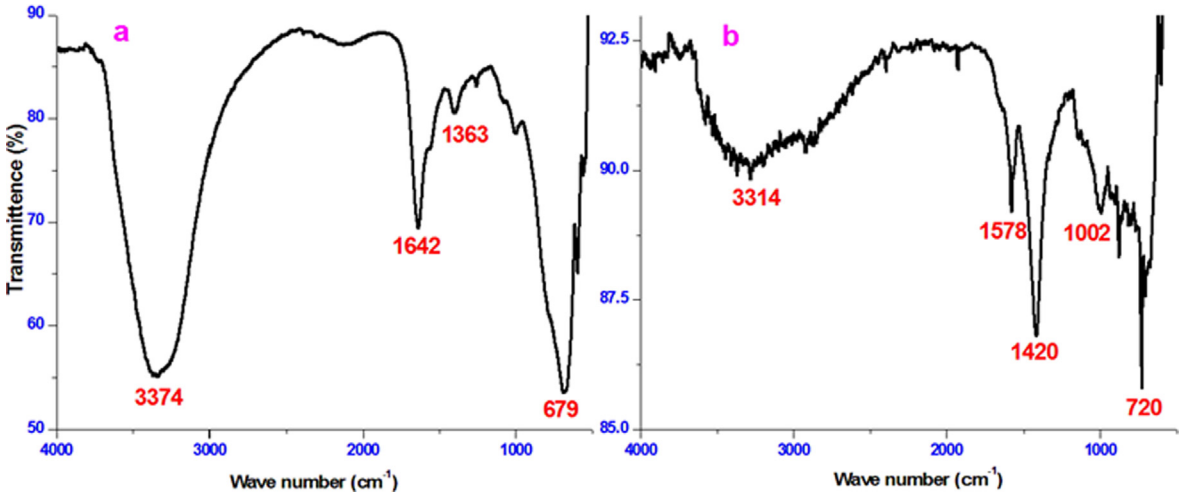

Fig. 8 FT-IR spectrum of mild steel in 1 mol/L HCl in the absence and presence of 100 ppm of HHR.

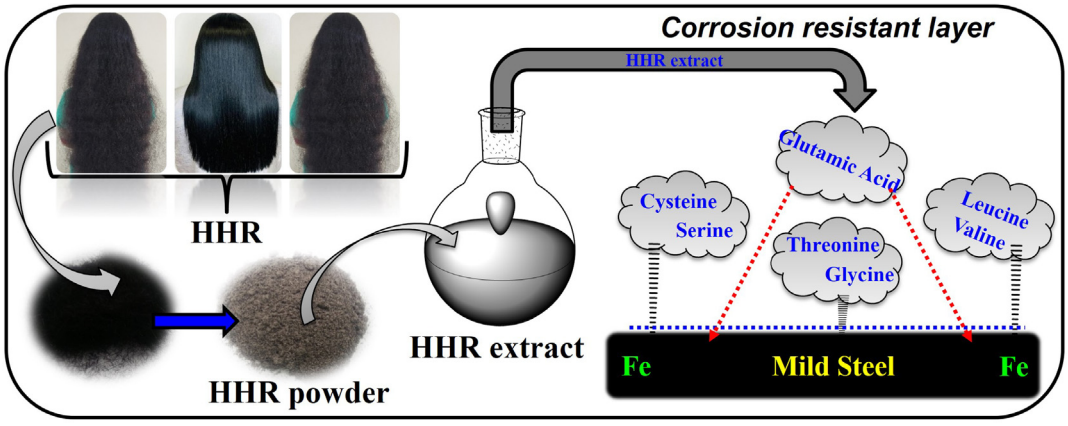

Fig. 9 Schematic diagram and possible mechanism of corrosion inhibition with HHR.

are adsorbed via donor-acceptor interactions between the free electron pairs of the heteroatoms and the π electrons of the pyrrolic and indolic rings (Chung et al., 2020a–c). In HCl, chloride ions with a low degree of hydration are specifically adsorbed on the steel surface, and they create a net negative charge at the interface. This leads to the strong adsorption of cationic inhibitor components via electrostatic interactions between the cationic HHR species and the chloride anions already adsorbed on the steel surface and hence greater efficiency (Fig. 9).

4. Conclusion

HHR extract containing the nontoxic pigment melanin, a nontoxic biopolymer, and lipids was obtained using a mixture of methanol, ethanol, and chloroform (40:30:30 v/v). HHR suppressed steel corrosion in 1 mol/L HCl at all the studied HHR concentrations and temperatures. The efficiency increased with increasing HHR concentration, but decreased with increasing temperature. The retardation of the corrosion occurred via the blockage of the active sites on the metal surface by the adsorption of the active components of HHR, which obeyed Langmuir isotherm. Gibbs free energy data for adsorption supported combined electrostatic and chemical adsorption. The temperature dependence of the efficiency of HHR was confirmed by the activation and thermodynamic parameters. Electrochemical results revealed that HHR can be classified as an effective mixed-type inhibitor for the corrosion of steel in 1 M HCl. Surface analysis using SEM-EDX and AFM observations confirmed the inhibition performance obtained gravimetrically and electrochemically, indicating the improved surface morphology of the metal due to a dense and ordered protective film of HHR formed on the steel surface. The FT-IR results also compliment the above conclusions. The results of the weight loss are in good agreement with electrochemical analysis.

Acknowledgments

This paper was supported by Konkuk University Research fund in 2017.

References

Abdallah, M., Megahed, H.E., Radwan, M.A., Abdfattah, E., 2012. Polyethylene glycol compounds as corrosion inhibitors for aluminum in 0.5 M hydrochloric acid solution. J. Am. Sci. 8, 49–55.

Abreu, C.M., Izquierdo, M., Merino, P., Nóvoa, X.R., Pérez, C., 1999. A new approach to the determination of the cathodic protection period in zinc-rich paints. Corrosion. 55, 1173–1181.

Afidah, A.R., Kassim, J., 2008. Recent development of vegetal tannins in corrosion protection of iron and steel. Recent Pat. Mater. Sci. 1, 223–231.

Akhtar, J.N., Ahmad, S., 2009. The effect of randomly oriented hair fiber on mechanical properties of fly-ash based hollow block for low height masonry structures. Asian J. Civ. Eng. 10, 221–228.

Ali, S.A., Al-Muallem, H.A., Saeed, M.T., Rahman, S.U., 2008. Hydrophobic-tailed bicycloisoxazolidines: A comparative study of the newly synthesized compounds on the inhibition of mild steel corrosion in hydrochloric and sulfuric acid media. Corros. Sci. 50, 664–675.

Al-Otaibi, M.S., Al-Mayouf, A.M., Khan, M., Mousa, A.A., Al-Mazroa, S.A., Alkhathlana, H.Z., 2014. Corrosion inhibitory action of some plant extracts on the corrosion of mild steel in acidic media. Arabian J. Chem. 7, 340–346.

Anadebe, V.C., Onukwuli, O.D., Omotioma, M., Okafor, N.A., 2018. Optimization and electrochemical study on the control of mild steel corrosion in hydrochloric acid solution with bitter kola leaf extract as inhibitor. S. Afr. J. Chem. 71, 51–61.

Anitha, R., Chitra, S., Hemapriya, V., Chung, I.M., Kim, S.H., Prabakaran, M., 2019. Implications of eco-addition inhibitor to mitigate corrosion in reinforced steel embedded in concrete. Constr. Build. Mater. 213, 246–256.

Anitha, R., Unnisa, C.B.N., Hemapriya, V., Roopan, S.M., Chitra, S., Chung, I.M., Kim, S.H., Prabakaran, M., 2020. Anti-corrosive potential of *Cyperus rotundus* as a viable corrosion inhibitor for mild steel in sulphuric acid. Pigment. Resin Technol. 49 (4), 295–304.

Antropov, L.I., 1967. A correlation between kinetics of corrosion and the mechanism of inhibition by organic compounds. Corros. Sci. 7, 607–620.

Atia, A.A., Saleh, M.M., 2003. Inhibition of acid corrosion of steel using cetylpyridinium chloride. J. Appl. Electrochem. 33, 171–177.

Baran, E., Cakir, A., Yazici, B., 2019. Inhibitory effect of *Gentiana olivieri* extracts on the corrosion of mild steel in 0.5 M HCl: Electrochemical and phytochemical evaluation. Arab. J. Chem. 12, 4303–4319.

Benarioua, M., Mihi, A., Bouzeghaia, N., Naoun, M., 2019. Mild steel corrosion inhibition by Parsley (*Petroselium Sativum*) extract in acidic media. Egypt. J. Pet. 28, 155–159.

Bentiss, F., Lagrenee, M., Traisnel, M., 2000. 2,5-Bis(n-Pyridyl)-1,3,4-Oxadiazoles as corrosion inhibitors for mild steel in acidic media. Corrosion. 56, 733–742.

Bockris, J.O.M., Swinkells, D.A.J., 1964. Adsorption of n-Decylamine on solid metal electrodes. J. Electrochem. Sci. 111, 736–743.

Chaitra, T.K., Mohana, K.N., Tandon, H.C., 2016. Study of new thiazole based pyridine derivatives as potential corrosion inhibitors for mild steel: theoretical and experimental approach. Int. J. Corros. 2016, 1–21.

Chitra, S., Chung, I.M., Kim, S.H., Prabakaran, M., 2019. A study on anticorrosive property of phenolic components from *Pachysandra terminalis* against low carbon steel corrosion in acidic medium. Pigment. Resin Technol. 48 (5), 389–396.

Chung, I.M., Hemapriya, V., Kanchana, P., Arunadevi, N., Chitra, S., Kim, S.H., Prabakaran, M., 2020a. Active-polyphenolic-compounds-rich green inhibitor for the surface protection of low carbon steel in acidic medium. Surf. Rev. Lett. 27 (6), 1950154.

Chung, I.M., Hemapriya, V., Ponnusamy, K., Arunadevi, N., Chitra, S., Chi, H.Y., Kim, S.H., Prabakaran, M., 2018. Assessment of low carbon steel corrosion inhibition by ecofriendly green *Chaenomeles sinensis* extract in acid medium. J. Electrochem. Sci. Technol. 9, 238–249.

Chung, I.M., Kim, S.H., Hemapriya, V., Kalaiselvi, K., Prabakaran, M., 2019. Inhibition behavior of *Tragia involucrata* L. phenolic compounds against acidic medium corrosion in low carbon steel surface. Chin. J. Chem. Eng. 27, 717–725.

Chung, I.M., Kim, S.H., Prabakaran, M., 2020b. Evaluation of phytochemical, polyphenol composition and anti-corrosion capacity of *Cucumis anguria* L. leaf extract on metal surface in sulfuric acid medium. Prot. Met. Phys. Chem. Surf. 56 (1), 214–224.

Chung, I.M., Malathy, R., Priyadharshini, R., Hemapriy, V., Kim, S. H., Prabakaran, M., 2020c. Inhibition of mild steel corrosion using Magnolia kobus extract in sulphuric acid medium. Mater. Today Commun. 25, 101687.

Deng, D., Gopiraman, M., Kim, S.H., Chung, I.M., Kim, I.S., 2016. Human hair: a suitable platform for catalytic nanoparticles. ACS Sustainable Chem. Eng. 4, 5409–5414.

Eroğlu, L., Guneren, E., Akbas, H., Demir, A., Uysal, A., 2003. Using human hair as suture material in microsurgical practice. J. Reconstr. Microsurg. 19, 37–39.

Farag, A.A., Ismail, A.S., Migahed, M.A., 2018. Environmental-friendly shrimp waste protein corrosion inhibitor for carbon steel in 1 M HCl solution. Egypt. J. Petrol. 27, 1187–1194.

Gopiraman, M., Deng, D., Zhang, K.Q., Kai, W., Chung, I.M., Karvembu, R., Kim, I.S., 2017. Utilization of human hair as a synergistic support for Ag, Au, Cu, Ni, and Ru nanoparticles: application in catalysis. Ind. Eng. Chem. Res. 56, 1926–1939.

Gupta, A., 2014. Human hair "waste" and its utilization: gaps and possibilities. J. Waste Manag. 2014, 1–17.

Gupta, C.S., 2008. Clay-traditional material for making handicrafts. Indian J. Tradit. Knowl. 7, 116–124.

Hassan, H.H., Abdelghani, E., Amin, M.A., 2007. Inhibition of mild steel corrosion in hydrochloric acid solution by triazole derivatives: Part I. Polarization and EIS studies. Electrochim. Acta 52, 6359–6366.

Hemapriya, V., Prabakaran, M., Parameswari, K., Chitra, S., Kim, S. H., Chung, I.M., 2017. Experimental and theoretical studies on inhibition of benzothiazines against corrosion of mild steel in acidic medium. Anti-Corros. Methods Mater. 64, 306–314.

Hemapriya, V., Prabakaran, M., Parameswari, K., Chitra, S., Kim, S. H., Chung, I.M., 2016. Dry and wet lab analysis on benzofused heterocyclic compounds as effective corrosion inhibitors for mild steel in acidic medium. J. Ind. Eng. Chem. 40, 106–117.

Hirao, Y., Ohkawa, K., Yamamoto, H., Fujii, T., 2005. A novel human hair protein fiber prepared by watery hybridization spinning. Macromol. Mater. Eng. 290, 165–171.

Jeeva, M., Venkatesa Prabhu, G., Rajesh, C.M., 2017. Inhibition effect of nicotinamide and its Mannich base derivatives on mild steel corrosion in HCl. J. Mater. Sci. 52, 12861–12888.

Ji, G., Anjum, S., Sundaram, S., Prakash, R., 2015. *Musa paradisica* peel extract as green corrosion inhibitor for mild steel in HCl solution. Corros. Sci. 90, 107–117.

Jmiai, A., ElIbrahimi, B., Tara, A., Oukhrib, R., El Issami, S., Jbara, O., Bazzi, L., Hilali, M., 2017. Chitosan as an eco-friendly inhibitor for copper corrosion in acidic medium: protocol and characterization. Cellulose 24, 3843–3867.

Karthik, R., Muthukrishnan, P., Chen, S.M., Jeyaprabha, B., Prakash, P., 2015. Anti-corrosion inhibition of mild steel in 1M hydrochloric acid solution by using *Tiliacora accuminata* leaves extract. Int. J. Electrochem. Sci. 10, 3707–3725.

Keleşoğlu, A., Yıldız, R., Ilyas Dehri, I., 2019. 1-(2-Hydroxyethyl)-2-imidazolidinone as corrosion inhibitor of mild steel in 0.5 M HCl solution: thermodynamic, electrochemical and theoretical studies. J. Adhes. Sci. Technol. 33 (18), 2010–2030.

Kumar, S.H., Karthikeyan, S., 2013. Torsemide and furosemide as green inhibitors for the corrosion of mild steel in hydrochloric acid medium. Ind. Eng. Chem. Res. 52, 7457–7469.

Lashgari, M., Arshadi, M.R., Biglar, M., 2010. Experimental and theoretical studies of media effects on copper corrosion in acidic environments containing 2-amino-5-mercapto-1,3,4-thiadiazole. J. Iran. Chem. Soc. 7, 478–486.

Liu, F.G., Du, M., Zhang, J., Qiu, M., 2009. Electrochemical behavior of Q235 steel in saltwater saturated with carbon dioxide based on new imidazoline derivative inhibitor. Corros. Sci. 51, 102–109.

Luo, X., Pan, X., Yuan, S., Du, S., Zhang, C., Liu, Y., 2017. Corrosion inhibition of mild steel in simulated seawater solution by a green eco-friendly mixture of glucomannan (GL) and bisquaternary ammonium salt (BQAS). Corros. Sci. 125, 139–151.

Lv, T.M., Zhu, S.H., Guo, L., Zhang, S.T., 2015. Experimental and theoretical investigation of indole as a corrosion inhibitor for mild steel in sulfuric acid solution. Res. Chem. Intermed. 41, 7073–7093.

Mahalakshmi, D., Unnisa, C.B.N., Hemapriya, V., Subramaniam, E. P., Roopan, S.M., Chitra, S., Chung, I.M., Kim, S.H., Prabakaran, M., 2019. Anticorrosive potential of ethanol extract of Delonix elata for mild steel in 0.5 M H_2SO_4 - a green approach. Bulg. Chem. Commun. 51 (1), 31–37.

Mahross, M.H., Naggar, A.H., Seaf Elnasr, T.A., Abdel-Hakim, M., 2016. Effect of rice straw extract as an environmental waste corrosion inhibitor on mild steel in an acidic media. Chem. Adv. Mater. 1, 6–16.

Malathy, R., Chung, I.M., Prabakaran, M., 2020. Characteristics of fly ash based concrete prepared with bio admixtures as internal curing agents. Constr. Build. Mater. 262, 120596.

Manokarana, G., Prabakaran, M., 2019. Evaluation of antioxidant and anticorrosion activities of *Ligularia fischeri* plant extract. Chem. Sci. Eng. Res. 1 (1), 16–24.

Mansfeld, F., Tsai, C.H., 1991. Determination of coating deterioration with EIS: I. Basic relationships. Corrosion 47, 958–963.

Mbonyiryivuze, A., Mwakikunga, B., Dhlamini, S.M., Maaza, M., 2015. Fourier transform infrared spectroscopy for sepia melanin. Phys. Mater. Chem. 3, 25–29.

Michael, D.P., Harish, S., Bensely, A., Lal, D.M., 2010. Insulation characteristics of sisal, human hair, coir, banana fiber composites at cryogenic temperatures. Polym. Renew. Resour. 1, 47–56.

Murthy, Z.V.P., Kaushik, G., Suratwala, R., 2004. Treatment of oily water with human hair as a medium: a preliminary study. Indian J. Chem. Technol. 11, 220–226.

Muthukrishnan, P., Jeyaprabha, B., Prakash, P., 2017. Adsorption and corrosion inhibiting behavior of *Lannea coromandelica* leaf extract on mild steel corrosion. Arab. J. Chem. 10, S2343–S2354.

Muthukrishnan, P., Saravana Kumar, K., Jeyaprabha, B., Prakash, P., 2014. Anticorrosive activity of *Kigelia pinnata* leaves extract on mild steel in acidic media. Metall. Mater. Trans. A 45, 4510–4524.

Nakamura, A., Arimoto, M., Takeuchi, K., Fujii, T., 2002. A rapid extraction procedure of human hair proteins and identification of phosphorylated species. Biol. Pharm. Bull. 25, 569–572.

Ocampo, L.B.M., Cisneros, M.G.V., Rodriguez, J.G.G., 2015. Using *Hibiscus sabdariffa* as corrosin inhibitor for Al in 0.5 M H_2SO_4. Int. J. Electrochem. Sci. 10, 388–403.

Oguzie, E.E., 2007. Corrosion inhibition of aluminium in acidic and alkaline media by *Sansevieria trifasciata* extract. Corros. Sci. 49 (2007), 1527–1539.

Oguzie, E.E., 2008. Corrosion inhibitive effect and adsorption behaviour of hibiscus sabdariffa extract on mild steel in acidic media. Port. Electrochim. Acta 26, 303–314.

Oguzie, E.E., Adindu, C.B., Enenebeaku, C.K., Ogukwe, C.E., Chidiebere, M.A., Oguzie, K.L., 2012. Natural products for materials protection: mechanism of corrosion inhibition of mild steel by acid extracts of *Piper guineense*. J. Phys. Chem. C 116, 13603–13615.

Prabakaran, M., Hemapriya, V., Kim, S.H., Chung, I.M., 2018. Evaluation of antioxidant and anticorrosion properties of *Epipremnum aureum*. Arab. J. Sci. Eng. 44, 169–178.

Prabakaran, M., Kim, S.H., Hemapriya, V., Chung, I.M., 2016a. Evaluation of polyphenol composition and anti-corrosion properties of *Cryptostegia grandiflora* plant extract on mild steel in acidic medium. J. Ind. Eng. Chem. 37, 47–56.

Prabakaran, M., Kim, S.H., Hemapriya, V., Chung, I.M., 2016b. *Tragia plukenetii* extract as an eco-friendly inhibitorfor mild steel corrosion in HCl 1 M acidic medium. Res. Chem. Intermed. 42 (2016d), 3703–3719.

Prabakaran, M., Kim, S.H., Hemapriya, V., Gopiraman, M., Kim, I. S., Chung, I.M., 2016c. *Rhus verniciflua* as a green corrosion inhibitor for mild steel in 1 M H2SO4. RSC Adv. 6, 57144–57153.

Prabakaran, M., Kim, S.H., Kalaiselvi, K., Hemapriya, V., Chung, I. M., 2016d. Highly efficient *Ligularia fischeri* green extract for the protection against corrosion of mild steel in acidic medium: Electrochemical and spectroscopic investigations. J. Taiwan Inst. Chem. Eng. 59, 553–562.

Prabakaran, M., Kim, S.H., Mugila, N., Hemapriya, V., Parameswari, K., Chitra, S., Chung, I.M., 2017. *Aster koraiensis* as nontoxic corrosion inhibitor for mild steel in sulfuric acid. J. Ind. Eng. Chem. 52, 235–242.

Rajeswari, V., Kesavan, D., Gopiraman, M., Viswanathamurthi, P., 2013. Physicochemical studies of glucose, gellan gum, and hydroxypropyl cellulose Inhibition of cast iron corrosion. Carbohydr. Polym. 95, 288–294.

Rajeswari, V., Kesavan, D., Gopiraman, M., Viswanathamurthi, P., Poonkuzhali, K., Palvannan, T., 2014. Corrosion inhibition of *Eleusine aegyptiaca* and *Croton rottleri* leaf extracts on cast iron surface in 1 M HCl medium. Appl. Surf. Sci. 314, 537–545.

Rehim, S.S.A.E., Ibrahim, M.A.M., Khalid, K.F., 2001. The inhibition of 4-(2′-amino-5′-methylphenylazo) antipyrine on corrosion of mild steel in HCl solution. Mater. Chem. Phys. 70, 268–273.

Saeed, M.T., Ali, S.A., Rahman, S.U., 2003. The cyclic hydroxylamines: a new class of corrosion inhibitors of carbon steel in acidic medium. Anti-Corros. Methods Mater. 50, 201–207.

Salasi, M., Sharabi, T., Roayaei, E., Aliofkhazraei, M., 2007. The electrochemical behaviour of environment-friendly inhibitors of silicate and phosphonate in corrosion control of carbon steel in soft water media. Mater. Chem. Phys. 104, 183–190.

Sangeetha, Y., Meenakshi, S., Sundaram, C.S., 2016. Corrosion inhibition of aminated hydroxyl ethyl cellulose on mild steel in acidic condition. Carbohydr. Polym. 150, 13–20.

Saranya, J., Sounthari, P., Chitra, S., 2017. Comparison of the inhibition property of Quinoxaline derivative on mild steel in 1.5M H_2SO_4, 3M HCl and 1M H_3PO_4. J. Mater. Environ. Sci. 8, 370–377.

Tan, B., Zhang, S., Liu, H., Guo, Y., Qiang, Y., Li, W., Guo, L., Xu, C., Chen, S., 2019. Corrosion inhibition of X65 steel in sulfuric acid by two food flavorants 2-isobutylthiazole and 1-(1,3-Thiazol-2-yl) ethanone as the green environmental corrosion inhibitors: Combination of experimental and theoretical researches. J. Colloid Interface Sci. 538, 519–529.

Tan, B., Zhang, S., Qiang, Y., Li, W., Li, H., Feng, L., Guo, L., Xu, C., Chen, S., Zhang, G., 2020. Experimental and theoretical studies on the inhibition properties of three diphenyl disulfide derivatives on copper corrosion in acid medium. J. Mol. Liq. 298, 111975.

Umoren, S.A., Eduok, U.M., Israel, A.U., Obot, I.B., Solomon, M. M., 2012. Coconut coir dust extract: a novel eco-friendly corrosion inhibitor for Al in HCl solutions. Green Chem. Lett. Rev. 5, 303–313.

Umoren, S.A., Gasem, Z.M., Obot, I.B., 2013. Natural products for material protection: inhibition of mild steel corrosion by date palm seed extracts in acidic media. Ind. Eng. Chem. Res. 52, 14855–14865.

Unnisa, C.B.N., Chitra, S., Devi, G.N., Kiruthika, A., Roopan, S.M., Hemapriya, V., Chung, I.M., Kim, S.H., Prabakaran, M., 2019. Electrochemical and nonelectrochemical analyses of cardo polyesters at the metal/0.5 M H_2SO_4 interface for corrosion protection. Res. Chem. Intermed. 45, 5425–5449.

Verma, A., Singh, V.K., Verma, S.K., Sharma, A., 2016. Human hair: A biodegradable composite fiber - a review. Int. J. Waste Resour. 6, 1–4.

Verma, D.K., Khan, F., 2016. Corrosion inhibition of mild steel in hydrochloric acid using extract of glycine max leaves. Res. Chem. Intermed. 42, 3489–3506.

Xu, J., Hu, C., Ji, Y., Hu, S., 2009. Ultrathin gold film deposited on human hair: Derivation from nanoparticles and applications as microsensors. Electrochem. Commun. 11, 764–767.

Yadav, M., Kumar, S., Sinha, R.R., Bahadur, I., Ebensobc, E.E., 2015. New pyrimidine derivatives as efficient organic inhibitors on mild steel corrosion in acidic medium: Electrochemical, SEM, EDX, AFM and DFT studies. J. Mol. Liq. 211, 135–145.

Yesudass, S., Olasunkanmi, L.O., Bahadur, I., Kabanda, M.M., Obot, I.B., Ebenso, E.E., 2016. Experimental and theoretical studies on some selected ionic liquids with different cations/anions as corrosion inhibitors for mild steel in acidic medium. J. Taiwan Inst. Chem. Eng. 64, 252–268.

Yildiz, R., Mer, B.D., 2019. Theoretical and experimental investigations on corrosion control of mild steel in hydrochloric acid solution by 4-aminothiophenol. Anti-Corros. Methods Mater. 66 (1), 127–137.

Yoo, B.Y., Shin, Y.H., Yoon, H.H., Seo, Y.K., Park, J.K., 2010. Hair follicular cell/organ culture in tissue engineering and regenerative medicine. Biochem. Eng. J. 48, 323–331.

Zhang, X., Zheng, Y., Wang, X., Yan, Y., Wu, W., 2014. Corrosion inhibition of N80 steel using novel diquaternary ammonium salts in 15% hydrochloric acid. Ind. Eng. Chem. Res. 53, 14199–14207.

Zheljazkov, V.D., Silva, J.L., Patel, M., 2008. Human hair as a nutrient source for horticultural crops. Hort. Technol. 18, 592–596.